CHARACTERIZATION OF ELASTOMERIC DIAPHRAGM MOTION IN A 12.88 INCH DIAMETER TANK UNDER 1-DOF SINUSOIDAL EXCITATION

J. Sargent [(1)], H. Gutierrez [(2)], D. Kirk [(3)], and W. Tam [(4)]

[(1-3)] Florida Institute of Technology, 150 W. University Blvd., Melbourne, FL 32901, sargent.joseph@gmail.com [(1)], hgutier@fit.edu [(2)], dkirk@fit.edu [(3)]
[(4)] ATK Space Systems, Inc., 6033 E. Bandini Blvd, Commerce, CA 90040, walter.tam@orbitalatk.com

KEYWORDS: Diaphragm tanks, slosh, linear stage

ABSTRACT:

The static shape and dynamic behavior of the diaphragm within a spacecraft or launch vehicle propellant tank must estimate the mass distribution of the vehicle to increase mission assuredness. The diaphragm may also undergo significant motion during ground transportation as well as when the vehicle is on the launch pad. Wind loading on the launch pad can cause excitations of the propellant tank and induce coupled diaphragm motion and propellant sloshing. Diaphragm weakening or failure (pull-out, rubbing against itself or the tank wall, tearing) can occur if the sloshing forces are sufficiently large. In this study a 12.88 inch diameter tank with an elastomeric diaphragm was subject to a lateral sinusoidal excitation motion to induce slosh for two diaphragms types (SIFA & AFE-332) with surrogate propellants of three different densities (1.02, 1.24, 1.30 g/cm^3) at three fill fractions (100%, 75%, & 50%) at three amplitudes set for three frequencies (1 Hz, 5 Hz, 10 Hz). Diaphragm displacement was measured under each of the different conditions. The majority of the cases exhibited little to no movement and correlated with visual observations.

1. INTRODUCTION

Elastomeric diaphragm tanks have been in use since the early stages of space flight as an effective means for propellant management [1-4]. Elastomeric diaphragm tanks utilize positive expulsion (pressure differential) for liquid propellant control and delivery. Positive expulsion devices include diaphragms, bladders, pistons or bellows-based systems. The two most practical types of spacecraft propulsion fluid control devices have proven to be diaphragms and bladders which contain elastomeric materials as an effective barrier between the pressurant gas and the liquid propellant. The majority of such tanks are used in monopropellant hydrazine systems, and most diaphragms are made using ATK's (formerly Pressure Systems, Inc.'s (PSI)) unique elastomeric reversing ethylene-propylene terpolymer (AFE-332) material. A typical elastomeric diaphragm tank assembly is shown in Figure 1.

In most cases the diaphragms are hemispherical or pill-shaped and clamped in place between the two halves of the propellant tank. Most diaphragms have ridges located on the propellant side to minimize propellant residual and the tank was designed to produce greater than 99.9% propellant expulsion; without these ribs, gas pockets might

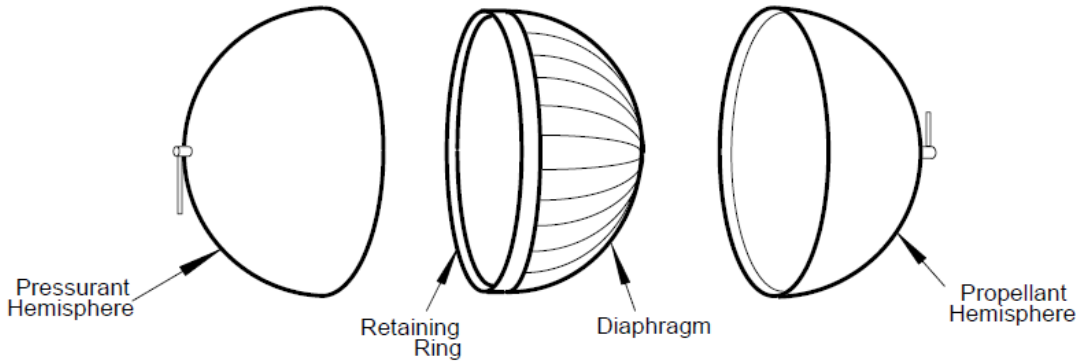

Figure 1. A typical elastomeric diaphragm tank assembly [3]

Figure 2. Example of 100%, 75% and 50% fill fractions (FF)

form to prevent propellant from reaching the outlet port.. Diaphragm tanks are typically easier to manufacture and have less severe folding patterns during operation than bladder tanks, whereas bladder tanks have a smaller sealing area and are easier to install, remove and replace as compared with diaphragm tanks [1].

Diaphragm rubbing is of particular concern in larger diameter tanks. For the ATK series of tanks, the elastomeric diaphragm material has the same thickness (0.07 inch) for all tanks with 9.4 to 40 inch diameter, corresponding to a diaphragm thickness, t, to diaphragm diameter, D, ratio of t/D = 0.00745 to 0.00175. This relative stiffness of the diaphragm is higher for the smaller diameter tanks and exhibits greater flexibility for the larger diameters.

In addition to diaphragm loading and potential pull-out problems during ground transportation, concerns also exist for having a more thorough knowledge of the diaphragms behavior once the vehicle is stacked and assembled waiting launch on the pad. For example, wind sway concerns for long, slender rockets are an important consideration. The spacecraft tank, which is located near the top of the vehicle, can experience a sinusoidal oscillation associated with the interaction of the wind with the launch vehicle. Oscillations frequencies of up to 3 Hz with several inches of lateral displacement may occur.

In order to achieve a better understanding of how wind conditions lead to diaphragm rub or excite natural slosh frequencies, a series of studies were performed using a 12.88 inch acrylic tank. Specifically, the objective of this study is to perform a range of tests with varying frequency and amplitude to produce different diaphragm loading conditions to determine the magnitude and frequency of the induced diaphragm motion during the simulated wind excitation.

Section 2 provides a description of the experimental set-up used to simulate on-pad wind sway environments. Section 3 presents the results and the findings of this study, and Section 4 presents a summary and conclusions.

1.1. Tank Description and Tank Slosh Overview

Experiments using ATK's 12.88 inch diameter acrylic simulator tank were performed at the Florida Institute of Technology's ***A***erospace ***S***ystems ***A***nd ***P***ropulsion (***ASAP***) Laboratory. The elastomeric diaphragm had a thickness of 0.07 inch, giving a t/D=0.0054 for the 12.88 inch tank. A detailed history of elastomeric diaphragm design, fabrication and testing, for tanks ranging from 9.4 to 40 inches in diameter, can be found in [4].

Examples of 100%, 75% and 50% fill fractions (FF) for the 12.88 inch tank are shown in Figure 2 to demonstrate that the diaphragm is relatively smooth and or contact with itself or the tank wall. In these examples, the propellant side is down and the pressurant side is up.

One of the objectives of this study was to understand and quantify the interaction between the diaphragm and the fluid motion within the tank as a result of excitations that occur during transportation, or while the vehicle is on the launch pad. Existing research on liquid sloshing within moving containers can be found in [7-9].

2. TESTS AND EXPERIMENTAL SET-UP

The tank provided by ATK was used to perform tests in accordance with the established test matrix shown in Table 1. The parameters in the test matrix were determined based on densities that were attainable, and commonly used fill fractions and frequencies in applications. A summary of these test cases can be seen in Figure 3.

The experimental setup included the tank mounted on a fully controllable 1-DOF motion table, as shown in Figure 4. The table uses linear bearings and is driven by a belt-system servomotor to move the tank and simulate the various environments that would create sloshing. To simulate different densities of fluid, sugar was added to water. The saturation limit of sugar in water is 1.33 (by weight) so this served as the limiting factor in determining the densities achievable by this method for testing.

A density of 1.46 g/cm^3 was requested, but unattainable using this method (1.30 g/cm^3 was tested instead). The density of each solution created was verified by measuring the weight of a sample of the liquid and dividing by the volume. The maximum volume the tank would fill was 14.825 liters or 3.92 gallons.

Table 1: Test Matrix

Diaphragms	Densities (g/cm^3)	Fill Fractions (%)	Frequency and Peak-to-peak Amplitude
SIFA & AFE-332	1.02 1.24 1.30	100 75 50	@ 1 Hz: 15 mm, 25 mm, 35 mm @ 5 Hz: 2.0 mm, 3.0 mm, 4.0 mm @ 10 Hz: 1.0 mm, 1.5 mm, 2.5 mm

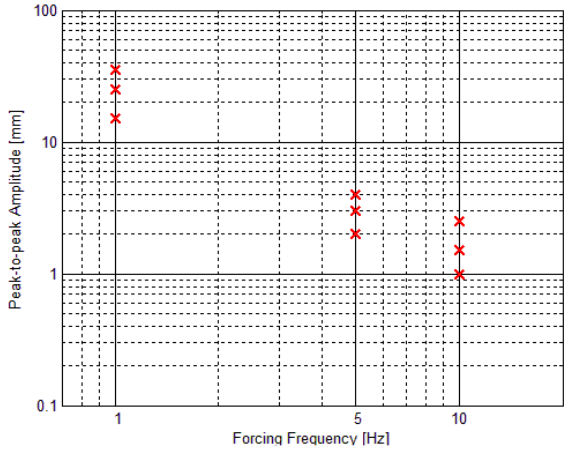

Figure 3. Summary of tests performed on the 12.88 inch simulator tank

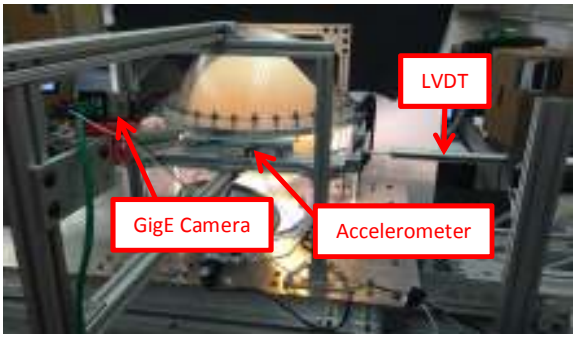

Figure 4. Experimental setup of 12.88 inch tank on 1-DOF table with belt-drive servomotor. Sensors depicted: GigE Camera, LVDT, accelerometer

LabVIEW was used to control the belt drive (Parker Model #:MPP1154B1E-KPSN, Serial #:081219N0009), shown on the left in Figure 4, for the 1 Hz and 5 Hz test cases. The 10 Hz excitation (right, Figure 4) was generated by a DSA-1K Power Amplifier by Data Physics. For all cases, light was added below the tank and a black background was used to try to increase the contrast of the membrane with its surroundings. Data collection was accomplished using:

- An iDS UI-5580CP-C-HQ GigE camera_at 34 frames per second (Part #: F1200AE, Serial #: 002) with computer lens (8mm 1:1.4)
- A Linear Variable Differential Transformer (LVDT) to measure relative displacement between the motor stage and tank table (Model: 060-3621-03, Serial #: L4137402, Range +/- 2.000 in)
- An accelerometer in the tank reference frame (Part #:060-6827-16, Serial #: 842573)

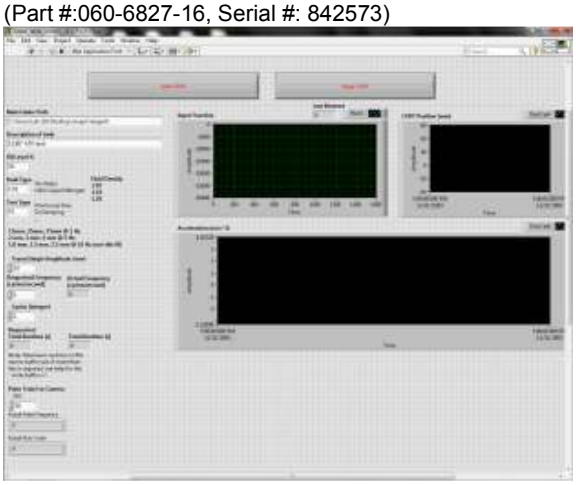

Figure 5. LabVIEW data collection system screenshot

The data collection for the accelerometer and LVDT data was accomplished using LabVIEW (**Error! Reference source not found.**) at 1.0 kHz and a separate computer for the image acquisition system with a SSD at 30 Hz. The image acquisition required a digitally triggered signal from LabVIEW to collect the data from the camera. The maximum frame rate was determined by the limitation of the camera (aperture and capture speed) in conjunction with the hard drive write speed for a given image size. The resolution of the images were 1280 x 960 pixels.

To determine the absolute membrane displacement, the midpoint of a bolt was measured to a point on the membrane. A subsection of the entire image was taken for a general crop and depicted in the upper left as "Area of Interest A." Then two more areas of interest were determined for both the membrane and a taller bolt. Motion of the bolt was observed relative to the image frame. Since the camera was mounted as an extension on the frame, the bolt is used as a reference to determine the displacement of the membrane relative to the tank and not just the membrane motion relative to the image. Next, both areas of interest's image contrast were adjusted independently until a clear distinction of the object was achieved. An edge detection algorithm determined the edge points.

For the bolt, the left side and right side of the bolt were determined by the greatest frequency of points along any x-location. 3 points to the left and right of the greatest frequency were then used and a weighted average was calculated for each side of the bolt. These weighted averages were then averaged to determine the center location of the bolt. Using this method, a precision of less than 0.5 pixels was determined when the tank was not in motion (~0.3 pixels on average). This compares to ~2.5 pixels using a measurement algorithm [10]. Note: Lighting situation was different and required an updated algorithm. Figure 6 provides an example of the algorithm breakout.

The membrane edge was estimated using a 2nd order polynomial and the y-intercept of this polynomial with the area of interest was used as the point to measure. The distance between the two was used to determine the absolute membrane

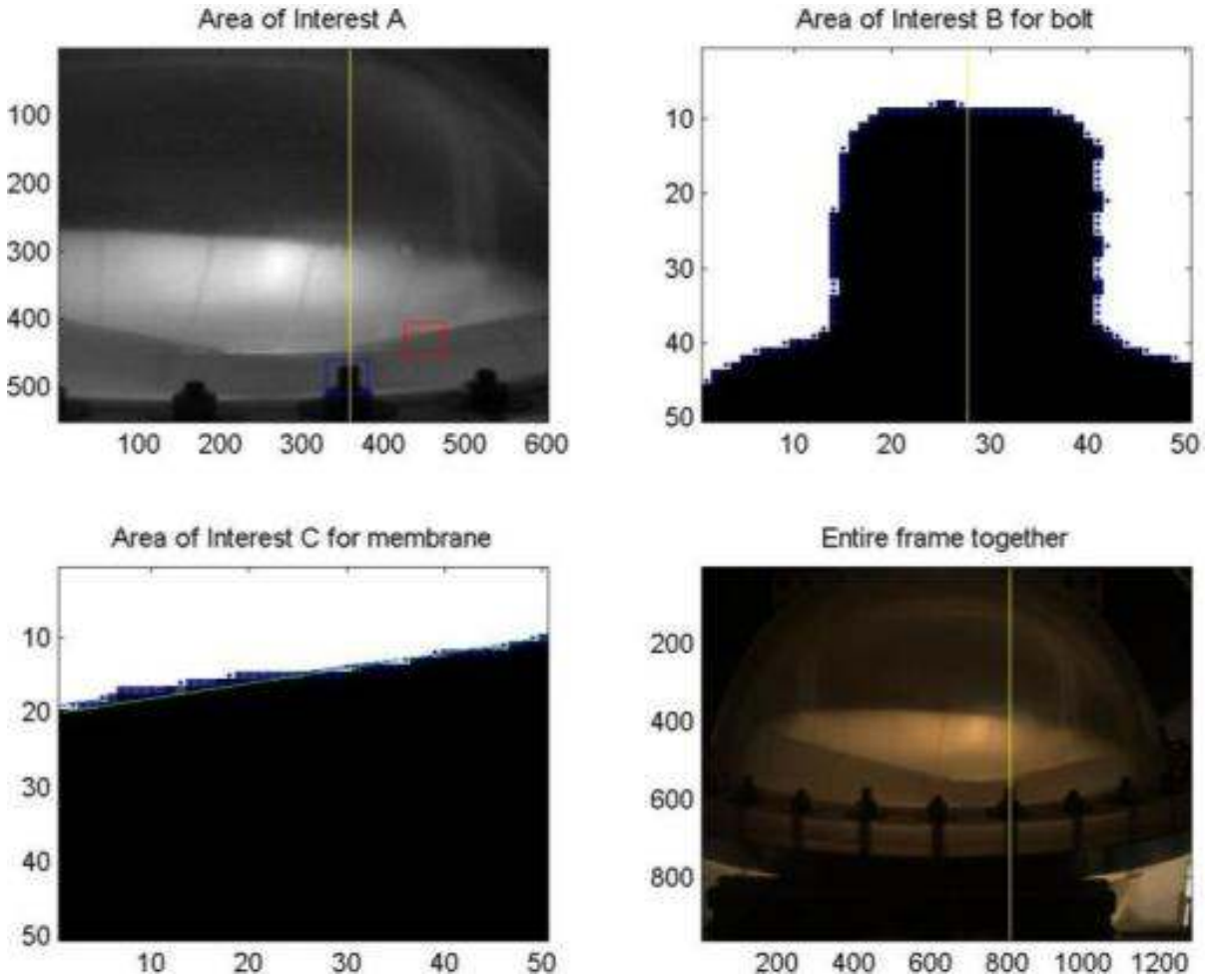

Figure 6. Example Algorithm Breakout

displacement. To convert from pixel displacement to a displacement in inches, a scaling factor of approximately 0.007912 inches per pixel was used.

3. RESULTS

An example of the absolute membrane displacement with the measured input acceleration and LDVT are depicted in Figure.7. For the 1 Hz and 5 Hz cases, a 0.5 second delay was used to allow the accelerometer to warm up. The figure shows good correlation between the measured excitation and measured membrane displacement. All tests with significant displacement followed the same behavior.

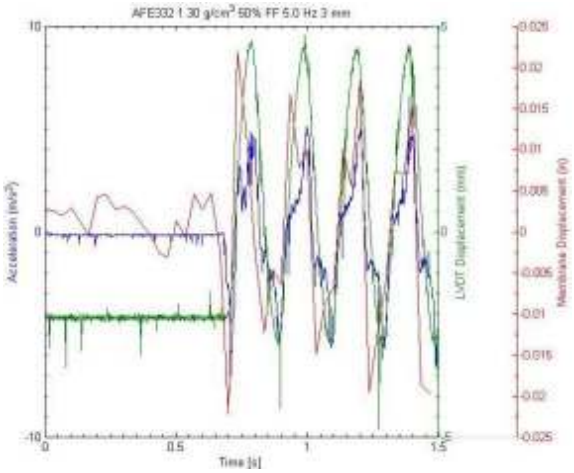

Figure.7 Example Accelerometer & LVDT feedback with membrane displacement

Table 2 summarizes the maximum membrane displacement for each test case. For example, the AFE332 - 1.30 g/cm^3 at 50% FF 5.0 Hz and 3 mm excitation had a maximum membrane displacement of 0.0256 in.

Since the resolution of the experiment is approximately 0.007912 inches per pixel, and the precision is 0.5 pixels, the minimum resolution is ~0.007912*0.5 = 0.003956 inches. This meant that any experiment with displacement less than or near this value was a result in algorithm 'noise'.

A graphical depiction of the previous table is provided on the next two pages. The goal was to determine which test cases exhibited the greatest membrane displacement. All frequencies and amplitudes are given for all tests corresponding to the each membrane and density combination. The larger the marker size, the higher the amplitude.

Table 2: Summary of Membrane Displacement for All Cases

Diaphragm	Density	Fill Fraction	Frequency and Amplitude (mm)				Max Displacement (respectively, in.)		
AFE-332	1.02 (g/cm^3)	50%	1.0 Hz	15	25	35	0.0041	0.0037	0.0038
			5.0 Hz	2	3	4	0.0045	0.0036	0.0051
			10 Hz	1.0	1.5	2.5	0.0041	0.0032	0.0056
AFE-332	1.02 (g/cm^3)	75%	1.0 Hz	15	25	35	0.0034	0.0032	0.0032
			5.0 Hz	2	3	4	0.0031	0.0038	0.0057
			10 Hz	1.0	1.5	2.5	0.0033	0.0037	0.0093
AFE-332	1.02 (g/cm^3)	100%	1.0 Hz	15	25	35	0.0037	0.0044	0.0045
			5.0 Hz	2	3	4	0.0037	0.0058	0.0077
			10 Hz	1.0	1.5	2.5	0.0041	0.0043	0.0046
AFE-332	1.24 (g/cm^3)	50%	1.0 Hz	15	25	35	0.0030	0.0034	0.0029
			5.0 Hz	2	3	4	0.0037	0.0063	0.0116
			10 Hz	1.0	1.5	2.5	0.0030	N/A[1]	0.0053
AFE-332	1.24 (g/cm^3)	75%	1.0 Hz	15	25	35	0.0077	0.0052	0.0063
			5.0 Hz	2	3	4	0.0063	0.0118	0.0180
			10 Hz	1.0	1.5	2.5	0.0110	0.0094	0.0111
AFE-332	1.24 (g/cm^3)	100%	1.0 Hz	15	25	35	0.0048	0.0051	0.0083
			5.0 Hz	2	3	4	0.0071	0.0125	0.0272
			10 Hz	1.0	1.5	2.5	0.0050	0.0074	0.0082
AFE-332	1.30 (g/cm^3)	50%	1.0 Hz	15	25	35	0.0095	0.0096	0.0152
			5.0 Hz	2	3	4	0.0201	0.0256	0.0298
			10 Hz	1.0	1.5	2.5	0.0271	0.0399	0.0576
AFE-332	1.30 (g/cm^3)	75%	1.0 Hz	15	25	35	0.0062	0.0050	0.0068
			5.0 Hz	2	3	4	0.0100	0.0168	0.0334
			10 Hz	1.0	1.5	2.5	0.0120	0.0298	0.0308
AFE-332	1.30 (g/cm^3)	100%	1.0 Hz	15	25	35	0.0090	0.0091	0.0099
			5.0 Hz	2	3	4	0.0095	0.0150	0.0531
			10 Hz	1.0	1.5	2.5	0.0654	0.0485	0.0383
SIFA	1.02 (g/cm^3)	50%	1.0 Hz	15	25	35	0.0029	0.0035	0.0057
			5.0 Hz	2	3	4	0.0042	0.0216	0.0045
			10 Hz	1.0	1.5	2.5	0.0028	0.0043	0.0036
SIFA	1.02 (g/cm^3)	75%	1.0 Hz	15	25	35	0.0029	0.0028	0.0040
			5.0 Hz	2	3	4	0.0028	0.0059	0.0092
			10 Hz	1.0	1.5	2.5	0.0044	0.0053	0.0065
SIFA	1.02 (g/cm^3)	100%	1.0 Hz	15	25	35	0.0030	0.0041	0.0035
			5.0 Hz	2	3	4	0.0033	0.0062	0.0126
			10 Hz	1.0	1.5	2.5	0.0041	0.0043	0.0079
SIFA	1.24 (g/cm^3)	50%	1.0 Hz	15	25	35	0.0079	0.0079	0.0104
			5.0 Hz	2	3	4	0.0121	0.0185	0.0247
			10 Hz	1.0	1.5	2.5	0.0261	0.0254	0.0143
SIFA	1.24 (g/cm^3)	75%	1.0 Hz	15	25	35	0.0050	0.0058	0.0072
			5.0 Hz	2	3	4	0.0131	0.0219	0.0306
			10 Hz	1.0	1.5	2.5	0.0114	0.0218	0.0343
SIFA	1.24 (g/cm^3)	100%	1.0 Hz	15	25	35	0.0075	0.0063	0.0114
			5.0 Hz	2	3	4	0.0087	0.0105	0.0197
			10 Hz	1.0	1.5	2.5	0.0066	N/A[2]	0.0109
SIFA	1.30 (g/cm^3)	50%	1.0 Hz	15	25	35	0.0134	0.0074	0.0114
			5.0 Hz	2	3	4	0.0210	0.0289	0.0403
			10 Hz	1.0	1.5	2.5	0.0284	0.0287	0.0355
SIFA	1.30 (g/cm^3)	75%	1.0 Hz	15	25	35	0.0072	0.0058	0.0083
			5.0 Hz	2	3	4	0.0191	0.0374	0.0491
			10 Hz	1.0	1.5	2.5	0.0189	0.0191	0.0550
SIFA	1.30 (g/cm^3)	100%	1.0 Hz	15	25	35	0.0139	0.0139	0.0094
			5.0 Hz	2	3	4	0.0127	0.0224	0.0271
			10 Hz	1.0	1.5	2.5	0.0315	0.1004	0.0308

[1] Data was corrupted from file transfer
[2] Data was corrupted from file transfer

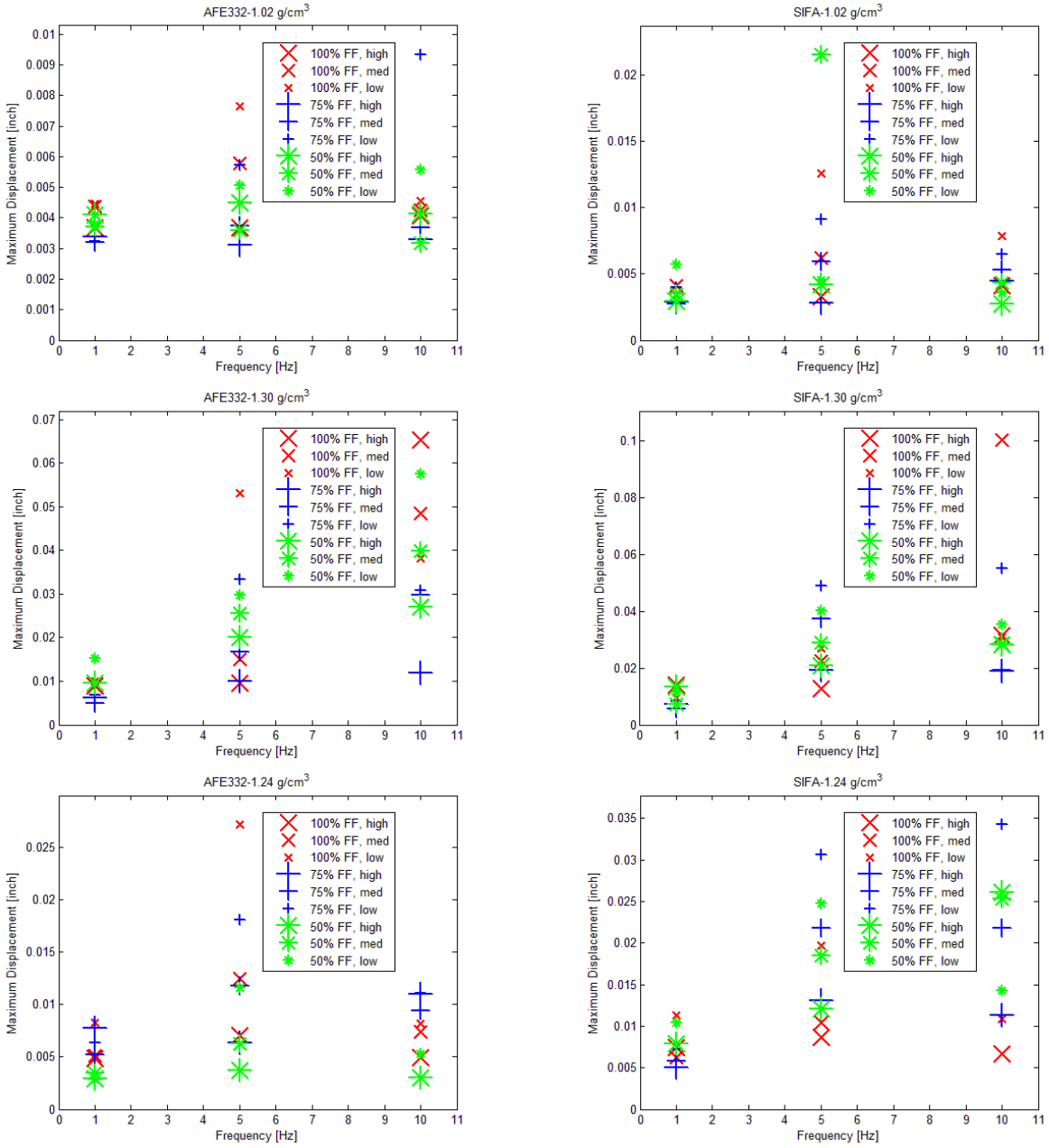

Note: The larger the marker, the higher amplitude of the experiment.

AFE332-1.24 g/cm^3-10 Hz-2.5 mm data corrupted

Note: The larger the marker, the higher amplitude of the experiment.

SIFA-1.24 g/cm^3-10 Hz-2.5 mm data corrupted

Figure 8. Graphical Results of test matrix

Table 3: Summary of Comparison Videos Generated

Video Number	Same parameters	Different parameter
1-9	SIFA, Density, max amplitude at each frequency	Fill Fraction
10-18	AFE-332, Density, max amplitude at each frequency	Fill Fraction
19-27	AFE-332, fill fraction, max amplitude at each frequency	Density
28-36	SIFA, fill fraction, max amplitude at each frequency	Density
37-63	Density, Fill fraction, max amplitude at each frequency (Side by side comparison)	Membrane

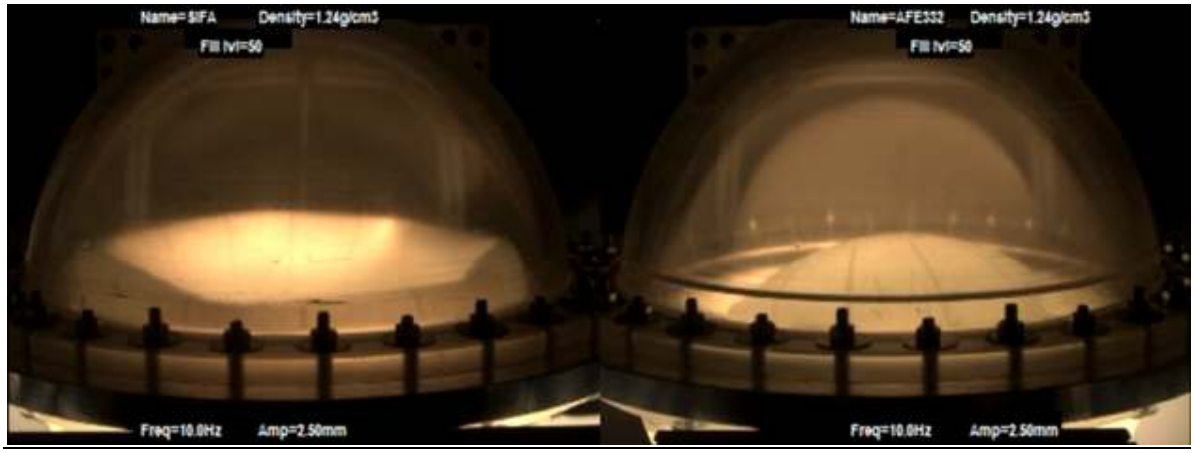

Figure 9. Example side-by-side comparison video

By changing one variable at a time, namely: diaphragm, density, fill fraction and frequency at maximum amplitude, videos were generated for side by side comparison as summarized in Table 3: Summary of Comparison Videos Generated. Figure 9 provides a sample image of the side by side comparison videos generated.

4. CONCLUSIONS

Diaphragm displacement was accurately measured with varying diaphragms, densities, fill fractions and excitation forces (frequency and amplitudes). The majority of the cases exhibited little to no movement and correlated with visual observations. The following observations were noted:

- Motion of the membrane was observed, in particular the higher frequencies with lower fill fractions
- In general, the low frequency test for all scenarios produced the least membrane displacement.
- The 100% fill fraction exhibited the least displacement for the lower two densities, but not for the largest density. This result could be from stretching the membrane with the higher density which would produce greater forces.
- Both membranes exhibited folding with 1.30 g/cm^3 density, but only the SIFA membrane 'folded' for 1.24 g/cm^3 and AFE332 did not. Both membranes did not fold with the 1.02 g/cm^3 density. It is unclear if this is due to the actual density or due to the surface tension between the membrane and the sugar water fluid itself.

5. FUTURE WORK

The membrane displacement was estimated with a single point on the diaphragm. Further measurements can be taken on the image sequences (i.e. measurement of the polynomial estimate to the line for all points or determining the membrane profile (see Figure) and determine membrane displacement relative to initial condition). There might be particular interest to

generate more data for specific situations from either the videos, tables or graphs.

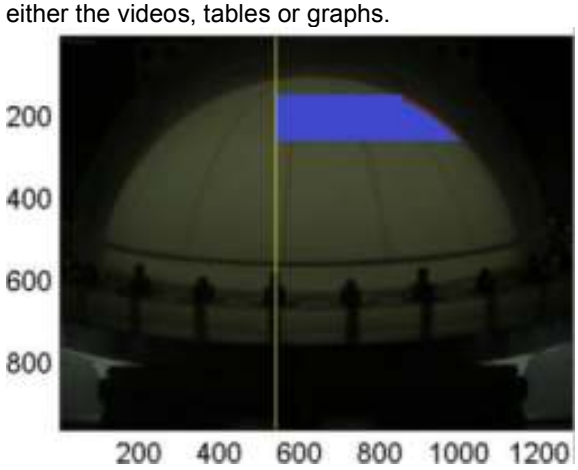

Figure 10. Proposed measurement image 1

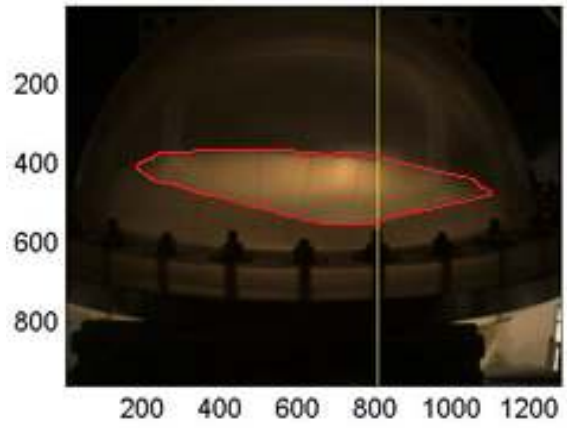

Figure 11. Proposed measurement image 2

6. REFERENCES

1. Brown, C. D., Spacecraft Propulsion, AIAA, Washington, 1995.

2. Sutton, G. P. & Biblarz, O., Rocket Propulsion Elements, John Wiley & Sons, New York, 2001.

3. Ballinger, I. A., Lay W. D., and Tam, W. H., "Review and History of PSI Elastomeric Diaphragm Tanks," AIAA 95-2534, 31st AIAA/ASME/SAE/ASEE Joint Propulsion Conference, San Diego, CA 1995.

4. Tam, W. H. and Taylor J. R., "Design and Manufacture of a Propellant Tank Assembly," AIAA 97-2813, 33rd AIAA/ASME/SAE/ASEE Joint Propulsion Conference, Seattle, WA 1997.

5. Kana, D. D. and Dodge, F. T., "Study of Liquid Slosh in the Tracking and Data Relay Satellite Hydrazine Tanks," Final Report SwRI Project 02-6539 under Contract NAS5-26482, CR 166745, Prepared for NASA Goddard Space Flight Center, September 25, 1981.

6. Dodge, F. T., The New Dynamic Behavior of Liquids in Moving Containers, Southwest Research Institute, San Antonio, TX, 2000.

7. Vergalla, M., Zhou, R., Gutierrez, H., and Kirk, D., "Experimental and Numerical Framework for Characterization of Slosh Dynamics," International Review of Aerospace Engineering, ISSN 1973-7459, Vol. 2. N. 1, pp. 52-61, February 2009.

8. Faure, J., Vergalla, M., Zhou, R., Chintalapati, S., Gutierrez, H., and Kirk, D., "Experimental Platform for the Study of Liquid Slosh dynamics Using Sounding Rockets," International Review of Aerospace Engineering, ISSN 1973-7459, Vol. 3, N. 1, pp. 59-67, February 2010.

9. Zhou, R., Vergalla, M., Chintalapati, S., Gutierrez, H., and Kirk, D. R., "Experimental and Numerical Investigation of Liquid Slosh Behavior Using Ground-based Platforms," AIAA Journal of Spacecraft and Rockets, Vol. 49, No. 6, November-December 2012.

10. Lapilli, G., Gutierrez H., and Kirk, D. R., "Characterization of Elastomeric Diaphragm Motion within a Spacecraft Propellant Tank," AIAA Joint Propulsion Conference, July 2015.